

Original Article

Exploring the antitumor effect of curcumin-piperlongumine hybrid molecule (CP) on EGFR-TKI-resistant non-small cell lung cancer using network pharmacological analysis and experimental verification

Shiyu Wang^{1,†}, Yinshuang Lai^{2,†}, Huijing Huang³, Jing Yuan¹, Shanxin Li⁴, Min Hui², Peipei Wang², Bingbing Chen¹, Zhiguo Liu^{2,*}, Jianchang Qian^{1,*}, and Qianwen Zhang^{1,*}

¹School of Pharmaceutical Sciences, Wenzhou Medical University, Wenzhou 325035, China, ²Chemical Biology Research Center at School of Pharmaceutical Sciences, Wenzhou Medical University, Wenzhou 325035, China, ³Yueqing People's Hospital, Wenzhou 325035, China, and ⁴Department of Pharmacy, Changhai Hospital, Naval Medical University, Shanghai 200433, China [†]These authors contributed equally to this work.

Received 8 November 2024 Accepted 7 February 2025 Published 9 July 2025

Abstract

EGFR-tyrosine kinase inhibitor (TKI) therapy is the most effective targeted therapy for non-small cell lung cancer (NSCLC). However, drug resistance remains a significant factor in the failure of lung cancer therapy. In the present study, we utilize network pharmacology, molecular docking, *in vitro* and *in vivo* experiments to explore the targets and biological mechanisms of CP, a novel curcumin-piperlongumine hybrid molecule, in EGFR-TKI-resistant NSCLC cells. The results reveal that CP exhibits enhanced biological activity compared to its parent compounds. CP can effectively inhibit cell proliferation by arresting cell cycle in the G2/M phase and inducing apoptosis. Mechanistically, CP-induced apoptosis is partially mediated by PI3K/AKT signaling pathway. These findings highlight the potential of CP as a promising therapeutic agent for EGFR-TKI-resistant lung cancer therapy.

Key words non-small cell lung cancer, curcumin, piperlongumine, resistance, EGFR-TKI, PI3K/AKT pathway

Introduction

Lung cancer is the most commonly diagnosed cancer and remains the leading cause of cancer-related death throughout the world [1]. About 85% of lung cancer cases are non-small cell lung cancer (NSCLC) [2]. The epidermal growth factor receptor gene *EGFR* is one of the key driver genes in NSCLC. EGFR mutations often lead to abnormal activation of downstream pathways such as PI3K/AKT/mTOR and MAPK pathways, which promote the proliferation, differentiation and migration of tumor cells [3]. Approximately 20% of NSCLC patients harbor activating mutations in EGFR. The exon 19 deletions and the L858R point mutation comprise more than 90% of EGFR activating mutations [4]. According to current treatment guidelines, EGFR tyrosine kinase inhibitors (EGFR-TKIs) are the first-line treatment for advanced NSCLC patients with activating EGFR mutations. AZD9291 (osimertinib) is an irreversible third-

generation epidermal growth factor receptor tyrosine kinase inhibitor (EGFR-TKI), and exhibits high selectivity against activating EGFR mutations, especially the T790M mutation [5]. However, the occurrence of acquired resistance is inevitable. Patients who initially benefit from osimertinib have been found to eventually develop resistance after 18.9 months [6]. Therefore, there is an urgent need to develop novel treatment strategies against EGFR-TKI resistance for advanced NSCLC.

Previous studies have revealed that curcumin and piperlongumine possess good antitumor activity in many types of cancers [7–9]. In addition, curcumin and piperlongumine have been reported to be potent tyrosine kinase inhibitors. It has been suggested that curcumin possesses good anti-EGFR activity, and curcumin overcomes Lenvatinib resistance through suppression of PI3K/AKT pathway in hepatocellular carcinoma [10]. Furthermore, curcumin

^{*}Correspondence address. Tel: +86-577-86699892; E-mail: lzgcnu@163.com (Z.L.) / Tel: +86-577-86689710; E-mail: qianjc@wmu.edu.cn (J.Q.) / Tel: +86-577-86689710; E-mail: zgwlovelove@126.com (Q.Z.)

analogs could dramatically inhibit the expression and phosphorylation of EGFR and reverse the EGFR-TKI resistance in gefitinibresistant NSCLC [11,12]. Piperlongumine has also been revealed to suppress cell proliferation and angiogenesis of hepatocellular carcinoma via the EGF/EGFR axis [13]. Additionally, piperlongumine could overcome doxorubicin resistance in leukemia by suppressing the PI3K/AKT signaling pathway [14]. More importantly, piperlongumine could inhibit the phosphorylation of AKT, and reverse resistance to cisplatin in NSCLC [15]. In our previous study, we successfully synthesized a novel curcumin-piperlongumine hybrid molecule, CP [16]. Date revealed that CP exhibited enhanced structural stability and safety compared with its parent compounds in lung cancer cells. However, whether CP has better antitumor activity in EGFR-mutant NSCLC and overcome EGFR-TKI resistance is still unknown.

Network pharmacology approach has been widely applied in the study of various traditional Chinese medicine treatment [17–19]. It provides a novel network model of "multiple targets, multiple effects, and complex diseases" to investigate the potential mechanism of herbal compounds or natural products [20]. Moreover, network pharmacology affords a better understanding of the pathogenesis of diseases and new strategies for personalized treatment [21].

In the present study, we first utilized network pharmacology method to elucidate target genes and signaling pathways of CP and then further investigated the antitumor efficiency of CP on AZD9291-resistant NSCLC. This study may provide a potential therapeutic drug for EGFR-TKI-resistant lung cancer.

Materials and Methods

Materials

The curcumin-piperlongumine hybrid molecule CP was synthesized as previously described [16]. Curcumin (B20614) and Piperlongumine (B20090) were purchased from Shanghai Yuanye Biotechnology Co., Ltd. (Shanghai, China). Z-VAD-FMK was purchased from APExBIO (A1902; Houston, USA) and osimertinib (AZD9291) was purchased from Selleck (S7297; Houston, USA). Inhibitors were dissolved in DMSO to prepare 20 mM stock solutions and were diluted prior to the assays. Antibodies against Phospho-EGFR (3777), Phospho-AKT (Ser473) (4060), Phospho-GSK-3β (Ser9) (5558), Cleaved PARP (Asp214) (5625), cyclin B1 (4138), c-Myc (5605), and Phospho-Cdc2 (Tyr15) (4539) were obtained from Cell Signaling Technology (Boston, USA). Antibodies against Phospho-PI3K (Tyr467/199) (T40116), PI3K (T40115) were obtained from Abmart (Shanghai, China). Antibodies against EGFR (18986-1-AP), AKT (80816-1-RR), GSK-3β (22104-1-AP), Bax (50599-2-1g), and Bcl-2 (26593-1-AP) were obtained from Proteintech (Wuhan, China). Antibodies against GAPDH (AP0063) were obtained from Bioworld (Nanjing, China)

Candidate therapeutic targets for CP and EGFR-TKIresistant NSCLC

The structure of CP was obtained by using Chemdraw 22.0.0 software (PerkinElmer, Cambridge, USA). Then, the 2D structure of CP was uploaded to the Pharmmapper database (http://lilab-ecust.cn/pharmmapper/), Swiss Target Prediction database (https://www.swisstargetprediction.ch/), Super-PRED database (https://prediction.charite.de/index.php) and SEA database (https://sea16.docking.org/) to acquire the targets of CP. EGFR-TKI-resistant NSCLC-

related targets were searched from GeneCards database (https://www.genecards.org/).

Construction of the protein-protein interaction (PPI) network and the intersection between CP and EGFR-TKI-resistant NSCLC

The PPI network of intersection targets between CP and EGFR-TKI-resistant NSCLC was constructed from the String (https://string-db. org/). The minimum required interaction score, ranging from 0 to 1, was set to > 0.7. The PPI network was further calculated, core targets was identified and visual analyzed using Cytoscape 3.10.2 software (https://cytoscape.org/). Subsequently, hub genes were identified through cytoHubba analysis within the Cytoscape software platform. The intersection targets between the predicted CP targets and EGFR-TKI-resistant NSCLC-related genes were obtained and visualized via the Venn Diagrams platform (http://bioinformatics.psb.ugent.be/webtools/Venn/).

Gene ontology (GO) and Kyoto encyclopedia of genes and genomes (KEGG) enrichment analyses

The GO and KEGG pathway enrichment analyses of intersection targets were elucidated using DAVID Bioinformatics Resources database (https://david.ncifcrf.gov/). FDR < 0.05 and P < 0.05 were used as cutoff values, and visualization of KEGG enrichment was performed via the R4.4.1.

Verification of molecular docking analysis

The 3D protein conformations corresponding to key target genes were retrieved from the RCSB PDB database (https://www.rcsb.org/), and the 2D structure for CP was translated into a 3D structure using Chemdraw software (22.0.0). The PyMOL 3.0.4 software (Schrödinger LLC, Portland, USA) was used to remove water molecules and co-crystal ligands from the protein structure. The AutoDockTools 1.5.7 (the Scripps Research Institute, La Jolla, USA) was used to precondition the ligands and receptors and then perform molecular docking using AutoDock vina. The CP structures that interact with the target proteins were screened, the one with the lowest binding energy in the docking results was selected as the ligand, the receptor proteins were processed to form complexes and visualized by the PyMOL software. The ligand-receptor protein complexes were then analyzed by using Protein-Ligand Interaction Profiler (PLIP, https://projects.biotec.tu-dresden.de/plip-web/plip/ index) to investigate the interaction between selected ligand and receptor protein.

Cell culture

PC9 cell line was obtained from the European Collection of Cell Cultures (ECACC, Salisbury, UK). H292 and H441 cell lines were obtained from the Cell Bank of Chinese Academy of Sciences (Shanghai, China). To generate the AZD9291-resistant PC9 cell line (PC9R), cells were treated with 1 μ M AZD9291. After several days of growth, surviving cells formed colonies. The colonies were selected and maintained with 1 μ M AZD9291. All cell lines were cultured in a medium supplemented with 10% fetal bovine serum (FBS; Sigma, St. Louis, USA), 1% sodium pyruvate, and 1% penicillin/streptomycin solution and maintained at 37°C with 5% CO2.

Cell viability assay

Cells were seeded into 96-well plates and incubated with different

concentrations of AZD9291 (6, 2, 0.67, 0.22, 0.074, 0.025, 0.0082, and 0.0027 $\mu M)$ for 96 h or Cur, PL, and CP (60, 20, 6.67, 2.22, 0.74, 0.25, 0.082, and 0.027 $\mu M)$ for 72 h. Cell viability was then measured using MTS reagent (Promega, Madison, USA). The absorbance at 490 nm was determined using an enzyme-linked immunosorbent assay (ELISA) reader (Molecular Devices MX190, Sunnyvale, USA).

Clonogenic growth assay

Cells were seeded in 12-well plates at a density of 800 cells/well. Appropriate drugs were added after an additional 24 h. The cells were exposed to the drugs or DMSO for 10 days. After colony formation, cells were fixed with 95% ethanol for 20 min, stained with 0.5% crystal violet solution (Solarbio, Beijing, China) for 20 min, and the number of colonies were counted.

Cell cycle distribution and apoptosis analysis

Cells were seeded in 6-well plates (30% confluency) and exposed to drugs for 24 h. For cell cycle distribution analysis, cells were collected and fixed overnight at $4\,^{\circ}\text{C}$ with 70% ethanol, followed by staining with propidium iodide (50 µg/mL; Sigma) for 10 min. Cell apoptosis was assessed using the Annexin V-FITC Apoptosis Detection Kit (BD Biosciences, Franklin Lakes, USA) according to the manufacturer's instructions. Cell cycle distribution and apoptosis were analyzed with a flow cytometer (BD FACSCalibur, Franklin Lakes, USA).

Mitochondrial membrane potential assay

Cells were plated in a 12-well plate (30% confluency) and exposed to various concentrations of drugs for 24 h. The mitochondrial membrane potential was evaluated using the JC-1 Mitochondrial Membrane Potential Assay Kit (Beyotime Biotechnology, Shanghai, China) following the manufacturer's instructions. Images were captured using an inverted fluorescence microscope (Nikon, Tokyo, Japan).

Western blot analysis

For western blotting, cells were lysed in NuPAGE-LDS lysis buffer (Invitrogen, Carlsbad, USA). The protein samples were then subjected to 10% SDS-PAGE and subsequently transferred to 0.45 μM nitrocellulose membranes (PALL, New York, USA). The membranes were blocked for 2 h at room temperature using freshly prepared 5% non-fat milk and then incubated overnight at 4°C with various primary antibodies at a 1:1000 dilution. Membranes were then incubated with the corresponding HRP-conjugated secondary antibodies (1:10,000; Jackson, West Grove, USA) for 2 h. GAPDH was used as a loading control.

In vivo tumor growth inhibition

BALB/c nude mice (4–6 week) were purchased from Beijing Vital River Laboratory Animal Technology Co., Ltd. (Beijing, China). Mice were housed in the animal center under standard conditions at 20–22°C and 50%–60% humidity, with a 12 h light/dark cycle. All animal experiments were conducted in accordance with the "Chinese Animal Ethics Regulations and Guidelines, People's Republic of China" and approved by the Animal Ethics Committee of Wenzhou Medical University (Ethics No. XMS92022-0370).

PC9R cells (4×10^6) were injected subcutaneously into the right flank of mice. Tumors were staged at an initial volume of 80

 $\sim 150~\text{mm}^3$ and randomized into treatment groups (*n* = 8). The CP was formulated in DMSO-PEG300-Tween-80-saline (2: 8: 1: 9). Mice were intraperitoneally injected once daily. Tumor sizes were measured every three days using calipers until the end of the study. The tumor volume was calculated using the following formula: V = (L × W²)/2 (where V was volume, L was length, and W was width).

Histological analysis

The tumor tissues were harvested, fixed in 4% paraformaldehyde, dehydrated, and embedded in paraffin. Paraffin-embedded tissue samples were sectioned into 5-µm slices and stained with H&E Staining Kit (Beyotime Biotechnology, Shanghai, China).

For Ki-67 staining, tumor sections were deparaffinized, rehydrated, and permeabilized with 1% Triton X-100. Antigen retrieval was achieved by microwaving in 1 mM Tris/EDTA (pH 9.0) for 20 min, followed by blocking in 5% BSA in TBS with 0.3 M glycine, and then probed with anti-Ki-67 antibody (Abcam, Cambridge, UK).

For TUNEL staining, TUNEL assay was performed using an *In situ* Cell Death Detection kit (Roche Applied Science, Mannheim, Germany) according to the manufacturer's instructions. Briefly, tumor sections were incubated with nuclease-free proteinase K working solution for 10 min at 37°C and then for 60 min at 37°C with the TUNEL reaction mixture, and then the sections were stained with FITC.

Images were acquired using a Pannoramic 250 Flash Scanner (3DHISTECH, Budapest, Hungary) and analyzed using the ImageJ software (Media Cybernetics Inc., Bethesda, USA).

Statistical analysis

Data processing and statistical analyses were performed using Microsoft Excel and GraphPad Prism 8 software (GraphPad Software, San Diego, USA). Unless otherwise stated, all experimental data are expressed as the mean \pm standard deviation. Comparisons between groups were performed using *t*-tests or one-way ANOVA. P < 0.05 was considered statistically significant.

Results

CP and EGFR-TKI-resistant NSCLC-related target prediction

After overlapping, 495 targets of CP were obtained from Pharmmapper, SEA, Swiss Target Prediction and Super-PRED databases by removing overlapping targets. A total of 430 targets of EGFR-TKI-resistant NSCLC were obtained from the GeneCards database.

Construction of CP with EGFR-TKI-resistant NSCLC intersection targets network

A total of 414 nodes and 2234 edges were found in the PPI network, as shown in Figure 1A. These targets were screened respectively according to degree value, betweenness centrality (BC), and closeness centrality (CC). There were 46 targets with average BC (0.01), CC (0.31), and degree values higher than the average (11), as shown in Figure 1B. The top 20 key targets were EGFR, SRC, HSP90AA1, TNF, JUN, ESR1, PIK3R1, PIK3CA, HSP90AB1, GRB2, HIF1A, EP300, NFKB1, MAPK3, MAPK1, MMP9, CASP3, PIK3CB, TLR4 and JAK2, as shown in Supplementary Table S1.

Totally, 31 common targets (Figure 1C and Supplementary Table S2) were screened based on the Venn diagram, and the diagram of a network of CP with EGFR-TKI-resistant NSCLC targets (Figure 1D)

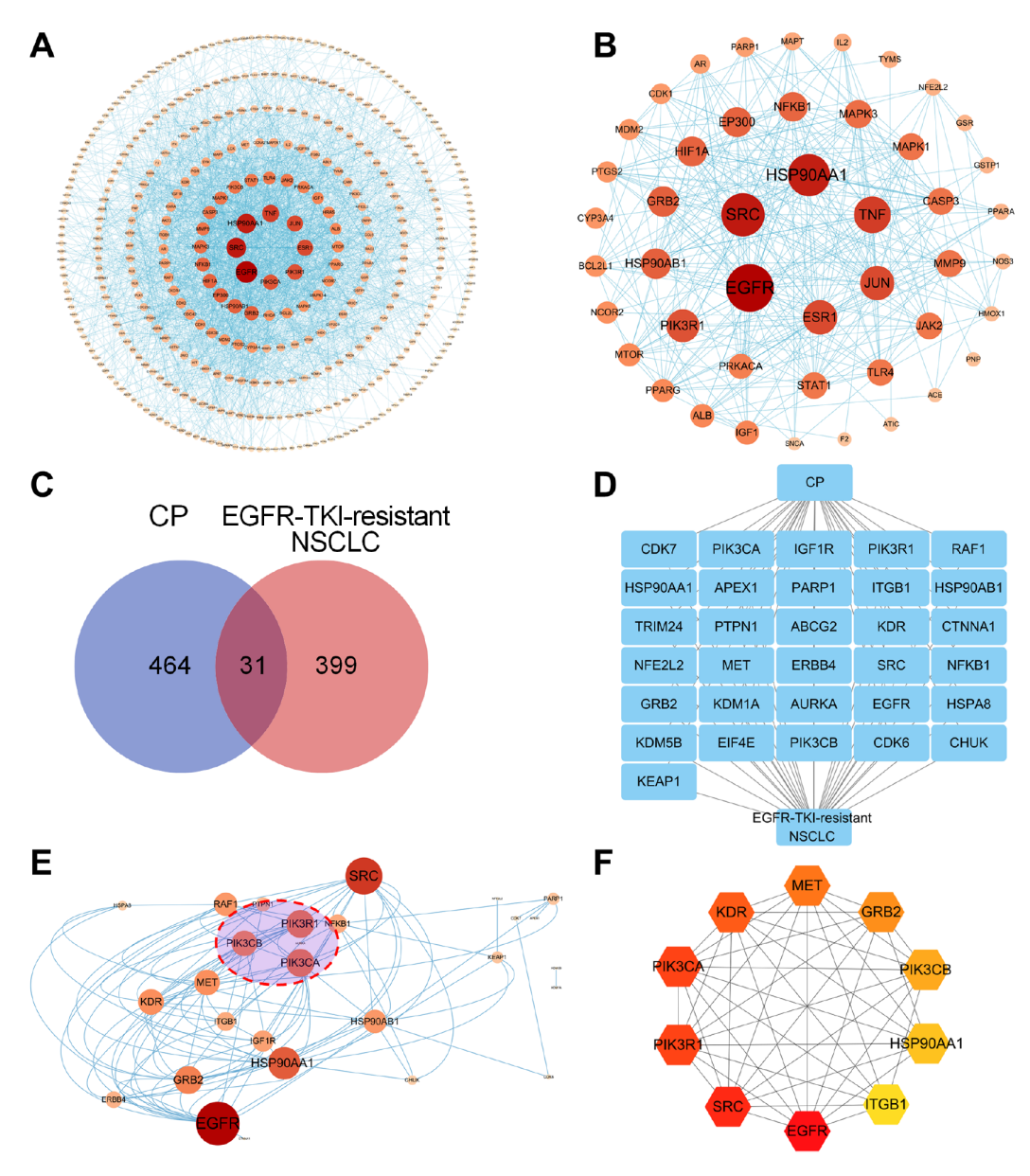


Figure 1. Identification of intersection targets shared by CP and EGFR-TKI-resistant NSCLC (A) A PPI network of CP-related targets. (B) The 46 core targets of CP with average BC, CC, and degree values higher than the average. The size of the nodes varies from small to large, the color varies from light brown to bottle brown, and the interactions increase gradually. (C,D) The 31 intersection targets of CP and EGFR-TKI-resistant NSCLC. (E) The PPI network of CP and EGFR-TKI-resistant NSCLC intersection targets. (F) Hubba targets of CP for treating EGFR-TKI-resistant NSCLC based on cytoHubba analysis.

was utilized using Cytoscape software. A total of 31 nodes and 102 edges were found, as shown in Figure 1E. These targets were filtered respectively according to cytoHubba analysis, and the hubba targets of CP for treating EGFR-TKI-resistant NSCLC were EGFR, SRC, PIK3R1, PIK3CA, KDR, MET, GRB2, PIK3CB, HSP90AA1, and ITGB1 (Figure 1F).

GO enrichment analysis and KEGG pathway annotation of CP-EGFR-TKI-resistant NSCLC intersection targets

After GO enrichment analysis, a total of 79 biological processes were obtained, including 33 biological processes (BP), 21 cellular components (CC), and 25 molecular function (MF) terms. The GO plot visualization of the top 5 items of BP, CC, and MF is shown in

Figure 2A. Among the enriched BP terms, the top five include the phosphorylation, negative regulation of apoptotic process phosphorylation, insulin receptor signaling pathway, insulin-like growth factor receptor signaling pathway and positive regulation of PI3K/AKT signal transduction. Enriched CC terms encompass the perinuclear region of perinuclear region of cytoplasm, cytosol, nucleoplasm, receptor complex, and nucleus. MF terms include ATP binding, insulin receptor substrate binding, transmembrane receptor protein tyrosine kinase activity, identical protein binding, and protein tyrosine kinase activity. To more intuitively identify the pathways associated with the targets, pathway information associated with the targets was obtained through KEGG analysis. KEGG enrichment analysis results revealed 118 potential pathways

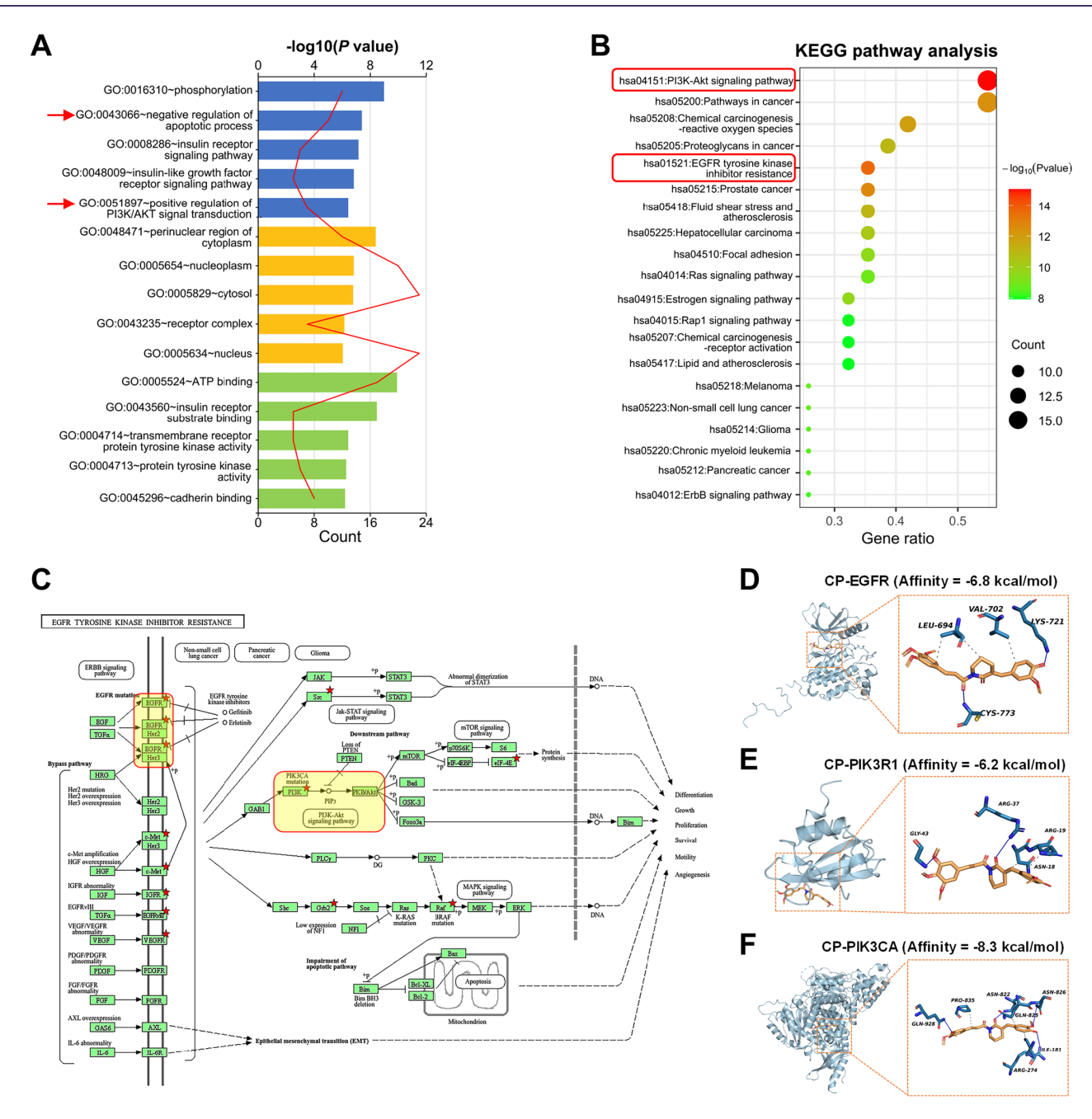


Figure 2. The enrichment analysis of CP-EGFR-TKI-resistant NSCLC common target proteins and validation of core targets (A,B) GO functional enrichment analysis (A) and KEGG pathway analysis (B) of CP in the treatment of EGFR-TKI-resistant NSCLC. (C) The key proteins and signaling pathways of the EGFR-TKI resistance signaling pathway. (D–F) Molecular docking of CP complexed with EGFR (D), PIK3R1 (E), and PIK3CA (F).

and the most significantly enriched 20 pathways are shown in Figure 2B. To investigate the therapeutic mechanism, we chose the classical PI3K-AKT signaling and EGFR tyrosine kinase inhibitor resistance pathway. Figure 2C shows the enrichment results of the intersecting targets in EGFR tyrosine kinase inhibitor resistance pathway.

Verification of CP and EGFR-TKI-resistant NSCLC by molecular docking analysis

To validate the findings of network pharmacology, we employed molecular docking to evaluate the interactions between the screened active drugs and targets. Based on the identified core targets, hub genes, and key pathways, we selected EGFR, PIK3R1 and PIK3CA for molecular docking with CP. In molecular docking, lower binding energies signify greater affinity and the likelihood of interaction. Analysis of the docking results revealed that the binding energies of CP and the corresponding proteins of the five core targets are less than –6 kcal/mol (Figure 2D–F), indicating that GP has the potential to bind to the receptor proteins of the 3 core targets. The binding affinities between them are mainly attributed to the abundant hydrogen bonding forces formed between the receptors and ligands.

Antiproliferative activity of CP on EGFR-TKI-resistant NSCLC cells

To investigate the anti-cancer effects of Cur, PL, and CP (Figure 3A) in NSCLC, we used human NSCLC cell lines H441, H292, PC9

(EGFR-mutant), and PC9-AZD9291-resistant (PC9R) cells. The data showed that PC9R cells were strongly resistant to AZD9291 (Figure 3B). MTS assay results showed that CP inhibited the proliferation of all 4 cell lines in a dose-dependent manner (Figure 3C,D and

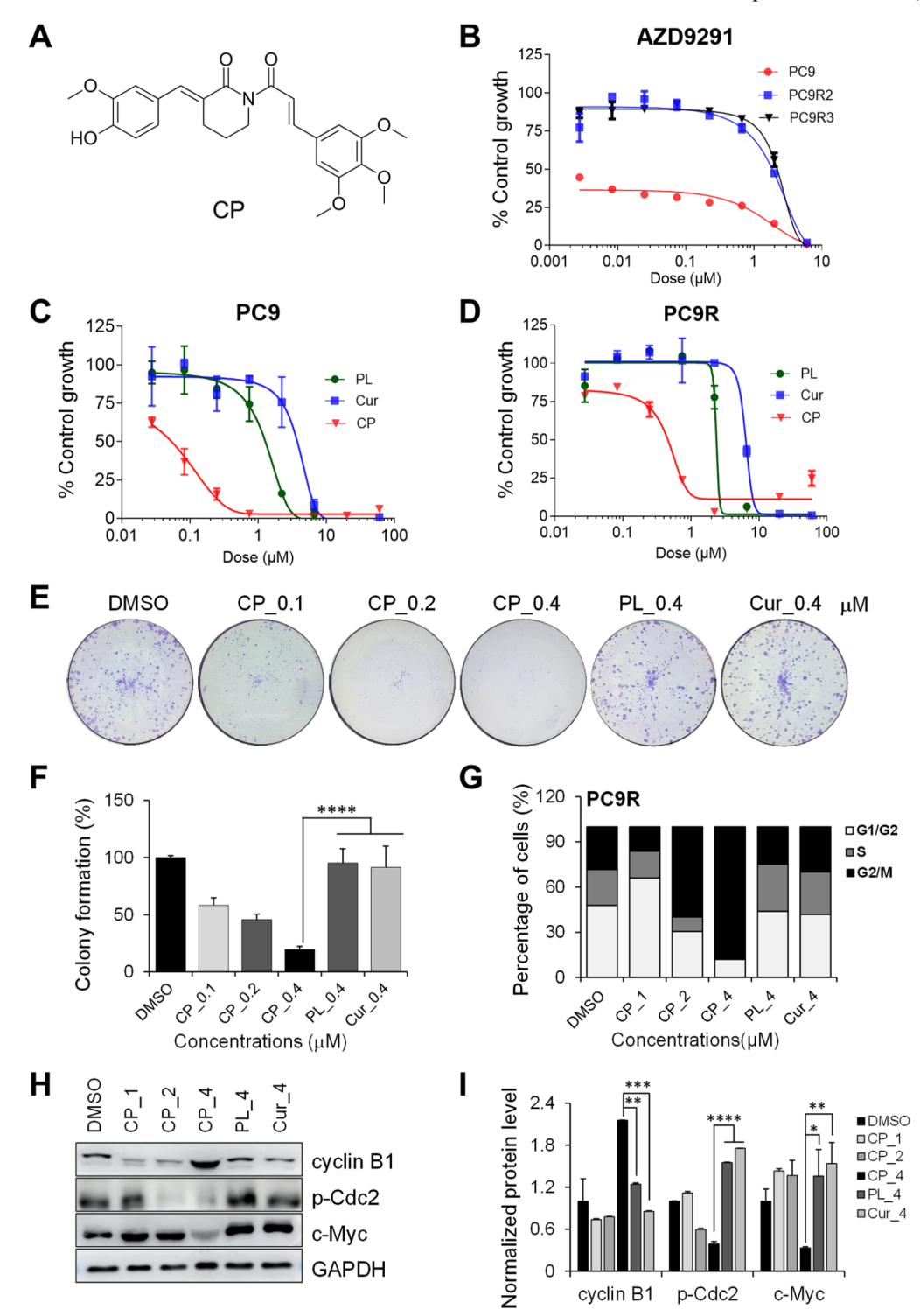


Figure 3. Antiproliferative activity of CP on EGFR-TKI-resistant cells (A) The chemical structure of CP was plotted. (B–D) The indicated cell lines were treated with various doses of AZD9291 (B) for 96 h or PL, Cur and CP (C and D) for 72 h, and the curves were plotted. (E) Colony formation assay in PC9R cells treated as indicated. (F) The quantified data of (E). (G) PC9R cells were treated as indicated for 24 h, then Pl staining analysis was conducted to analyze the cell cycle distribution by flow cytometry. (H) Cells were treated as indicated for 24 h and then subject to immunoblotting. (I) Quantified data of (H). *P<0.05; **P<0.01; ***P<0.001; ****P<0.0001.

Supplementary Figure S1A,B). In particular, CP demonstrated a relatively low IC₅₀ value (< 0.5 μ M) than PL (> 3.01 μ M) and Cur (> $6.44 \mu M$) (Table 1). Consistent with the results of cell viability, CP displayed superior inhibition of colony formation in PC9 (Supplementary Figure S1C,D) and PC9R (Figure 3E,F) cells compared to PL and Cur. Then the effect of CP on cell cycle progression was analyzed. As expected, CP treatment induced dose-dependent G2/M arrest in PC9 (Supplementary Figure S1E) and PC9R cells (Figure 3G), whereas PL and Cur had no significant effect on the cell cycle. Correspondingly, CP dose-dependently reduced the levels of cell cycle-related or cell proliferation-related p-Cdc2 and c-Myc in the PC9 (Supplementary Figure S1F) and PC9R cells (Figure 3H). Interestingly, CP treatment significantly increased cyclin B1 levels in PC9R cells (Figure 3I), but the increase in cyclin B1 level in PC9 cells was limited (Supplementary Figure S1G). Accordingly, PC9R cells exhibited a lower inhibition of the S population. During the G2 phase, the Cdc2-cyclin B1 complex receives the signal that DNA replication has been successfully completed and phosphorylates various cytoskeletal proteins and nuclear proteins, which is vital for G2/M transition and mitosis [22]. Cyclin B1 is believed to be essential for the progression through S phase and is active during G2/M transition [23,24]. Cdc-2 is necessary for entry into mitosis [25]. In consequence, treatment with CP caused the suppression of Cdc-2 phosphorylation, leading to G2/M cell cycle arrest in PC9 and PC9R cells. The decrease in the S population observed in CP-treated PC9R cells may be attributed to the activity of cyclin B1. Collectively, these results suggested that CP greatly inhibits the growth of EGFR-TKI-resistant lung cancer cells by inducing cell cycle arrest at the G2/M phase.

CP induces apoptosis in EGFR-TKI-resistant NSCLC cells

To further investigate the effects of CP on the physiological functions of PC9R cells, cell death was evaluated by flow cytometry. The results revealed that CP dose-dependently induced apoptosis in PC9 (Supplementary Figure S2A,C) and PC9R cells (Figure 4A,C). More importantly, the apoptosis rate in the CP group was higher than that in the PL or Cur groups at the same dose (4 μ M) in both cell lines. Mitochondrial damage is a key hallmark of apoptosis and is characterized by changes in mitochondrial transmembrane potential (MMP), leading to alterations in membrane permeability. To evaluate MMP integrity in the two cell lines after treatment, JC-1 $\,$ staining was employed. In healthy cells, the mitochondria form aggregates that emit intense red fluorescence. In apoptotic cells, mitochondria exist as monomers in the cytosol due to changes in MMP and emit green fluorescence. With an increase in CP concentration (1, 2, and 4 µM), there was a significant reduction in the ratio of red (JC-1 aggregates) to green (JC-1 monomers) fluorescence, indicating that CP induced MMP disruption in PC9 (Supplementary Figure S2B,D) and PC9R cells (Figure 4B,D). PARP, a molecule that responds to DNA damage, is cleaved and activated by caspase 3. Western blot analysis showed that CP induced PARP cleavage (CL-PARP) in a dose-dependent manner in both cell lines (Figure 4E,F and Supplementary Figure S2E,F). Furthermore, CPinduced apoptotic cell death was attenuated by Z-VAD-FMK, a cellpermeable pan-caspase inhibitor (Figure 4G,H), indicating that caspases are involved in CP-triggered apoptosis in PC9R cells. Taken together, these results demonstrated that CP induces apoptosis in EGFR-TKI-resistant NSCLC cells in a dose-dependent manner.

CP inhibits EGFR/PI3K/AKT signaling cascade in EGFR-TKI-resistant NSCLC cells

To determine the pathway contributing to CP-induced cell death in EGFR-TKI-resistant NSCLC cells, we performed western blot analysis on PC9R cells treated with or without CP. KEGG pathway enrichment analysis suggested that the most significant pathway affected by CP treatment is related to the PI3K/AKT pathway (Figure 2). Results showed that the expression levels of p-EGFR, p-PI3K, p-AKT, p-GSK-3 β were significantly reduced in the CP treatment group (Figure 5). These results highlight that the EGFR/PI3K/AKT cascade may play an important role in CP-induced anti-tumor effects in EGFR-TKI-resistant NSCLC cells.

CP prevents growth of EGFR-TKI-resistant lung cancer in xenograft tumors

We further investigated the therapeutic potential of CP in a xenograft lung cancer model. We observed a significant reduction in PC9R tumor growth following treatment with 50 mg/kg CP without any significant changes in body weight (Figure 6A,E). Histological analysis, including H&E, Ki-67, and TUNEL staining, revealed that the CP treatment group exhibited more prominent necrosis, decreased Ki-67-positive tumor cells, and increased TUNEL-positive cells compared to the control group (Figure 6B-D). Furthermore, western blot analysis demonstrated that CP treatment led to reduced expressions of p-EGFR, p-PI3K, p-AKT, p-GSK-3β, c-Myc, Bcl-2, while increasing cyclin B1, BAX expressions in the tumor tissues (Figure 6F,G). Among them, Bcl-2 is an anti-apoptotic protein, and Bax is a pro-apoptotic protein, indicating that CP can effectively induce the apoptosis of tumor cells. These findings indicate that CP exhibits promising anti-tumor activity against EGFR-TKI-resistant lung cancer at a safe dosage in vivo.

Discussion

The 3rd generation EGFR-TKIs such as AZD9291 (osimertinib) has remarkable clinical activity and tolerability. For patients who were treated with the 1st-generation EGFR-TKI and bear a T790M mutation, their PFS and OS time will be successfully improved after AZD9291 treatment compared with chemotherapy [26]. More importantly, in advanced NSCLC patients with EGFR mutations, AZD9291 showed greater activity and a lower rate of serious adverse events than gefitinib or erlotinib [6,27]. However, acquired resistance during long-term treatment have restricted its clinical application. In our previous study, CP was found to possess significantly stronger antitumor activity than curcumin and piperlongumine [16]. In this study, CP was found to effectively suppress the growth and induce cell apoptosis of EGFR-TKIresistant NSCLC cells. The underlying mechanisms is related to EGFR/PI3K/AKT signaling cascade. This study provides a theoretical basis for further exploring the efficacy and mechanism of action of CP.

Firstly, we used network pharmacology to investigate the potential mechanisms associated with CP for the treatment of EGFR-TKI-resistant NSCLC and screened 31 core targets of CP for the treatment of NSCLC. Core target enrichment analysis showed that the PI3K/AKT signaling pathway might be the core pathway for the treatment of EGFR-TKI-resistant NSCLC. After that, molecular docking was performed on the 3 core targets screened, and the results showed that a good relationship was established between CP and the core targets relying on the hydrogen bonding force.

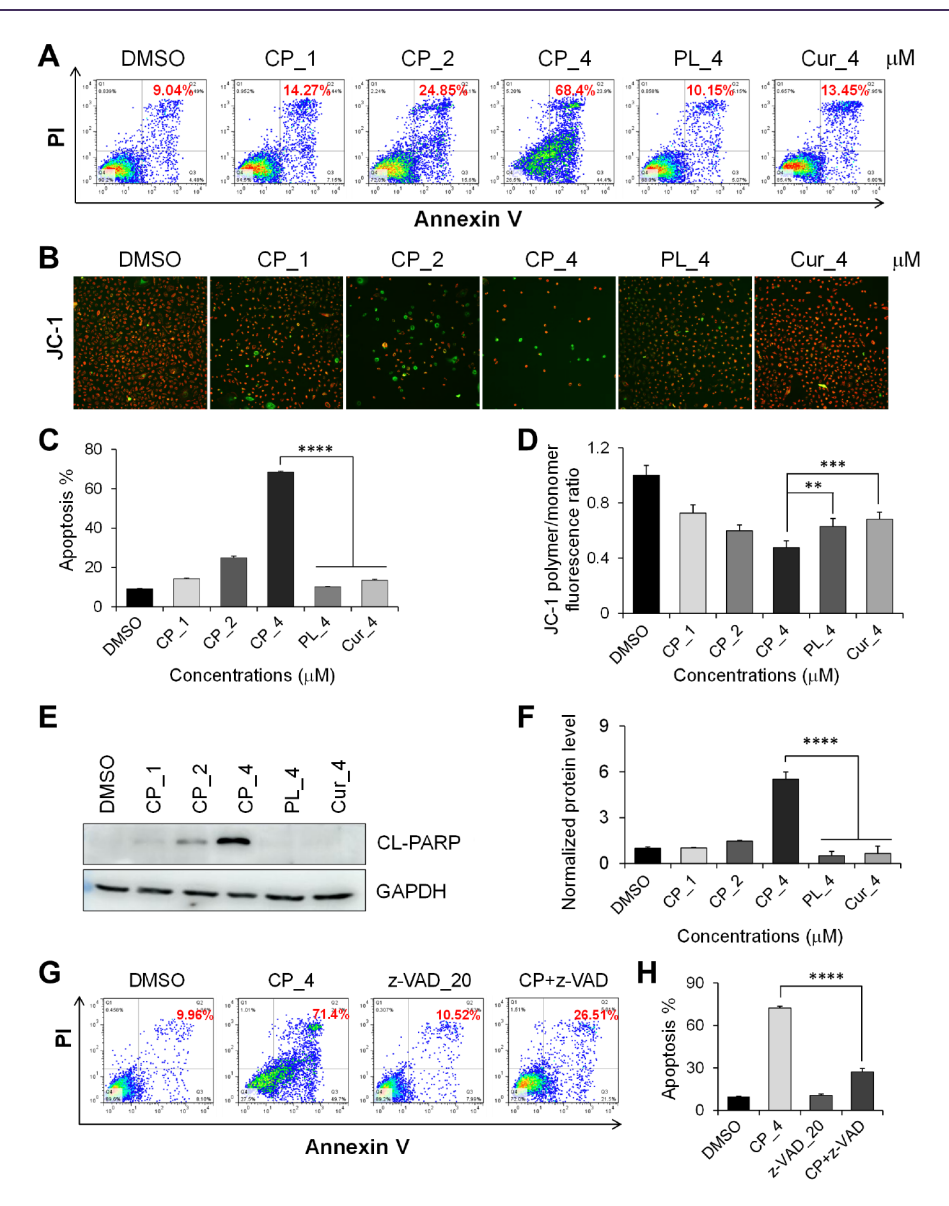


Figure 4. CP induces apoptosis in EGFR-TKI-resistant cells (A) Cells were exposed to CP, PL or Cur as indicated for 24 h, and Annexin V-FITC/Pl staining analysis was conducted to evaluate the apoptotic cells by flow cytometry. (B) JC-1 staining of apoptosis in PC9R cells (200x). (C,D) Quantified data of (A) and (B). (E) Cells were treated as indicated for 24 h and then subject to immunoblotting. (G) Cells were treated as indicated for 24 h after pretreatment with or without Z-VAD-FMK (20 μ M) for 2 h and then assayed using Annexin V-FITC/Pl staining kit. (F,H) Quantified results of (E) and (G). **P < 0.001; ***P < 0.001; ****P < 0.0001.

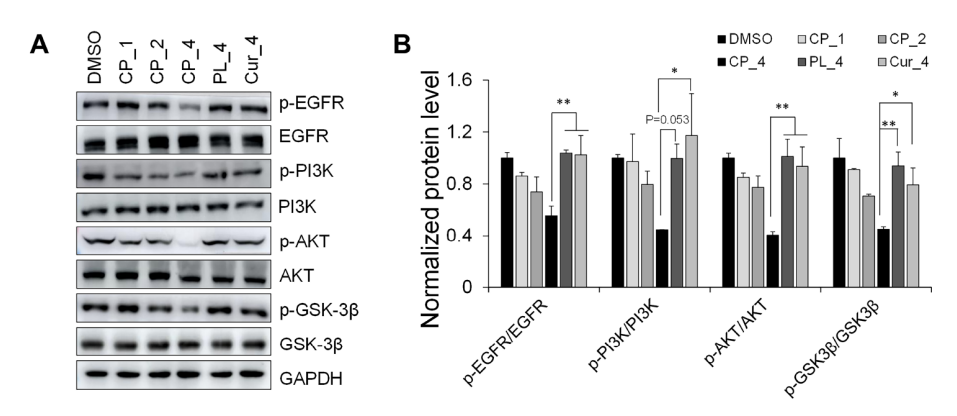


Figure 5. CP blocks the activation of PI3K/AKT/GSK-3 β cascade in EGFR-TKI-resistant NSCLC cells (A) Cells were treated as indicated for 24 h and then subject to immunoblotting. (B) Quantified results of (A). *P<0.05; **P<0.01.

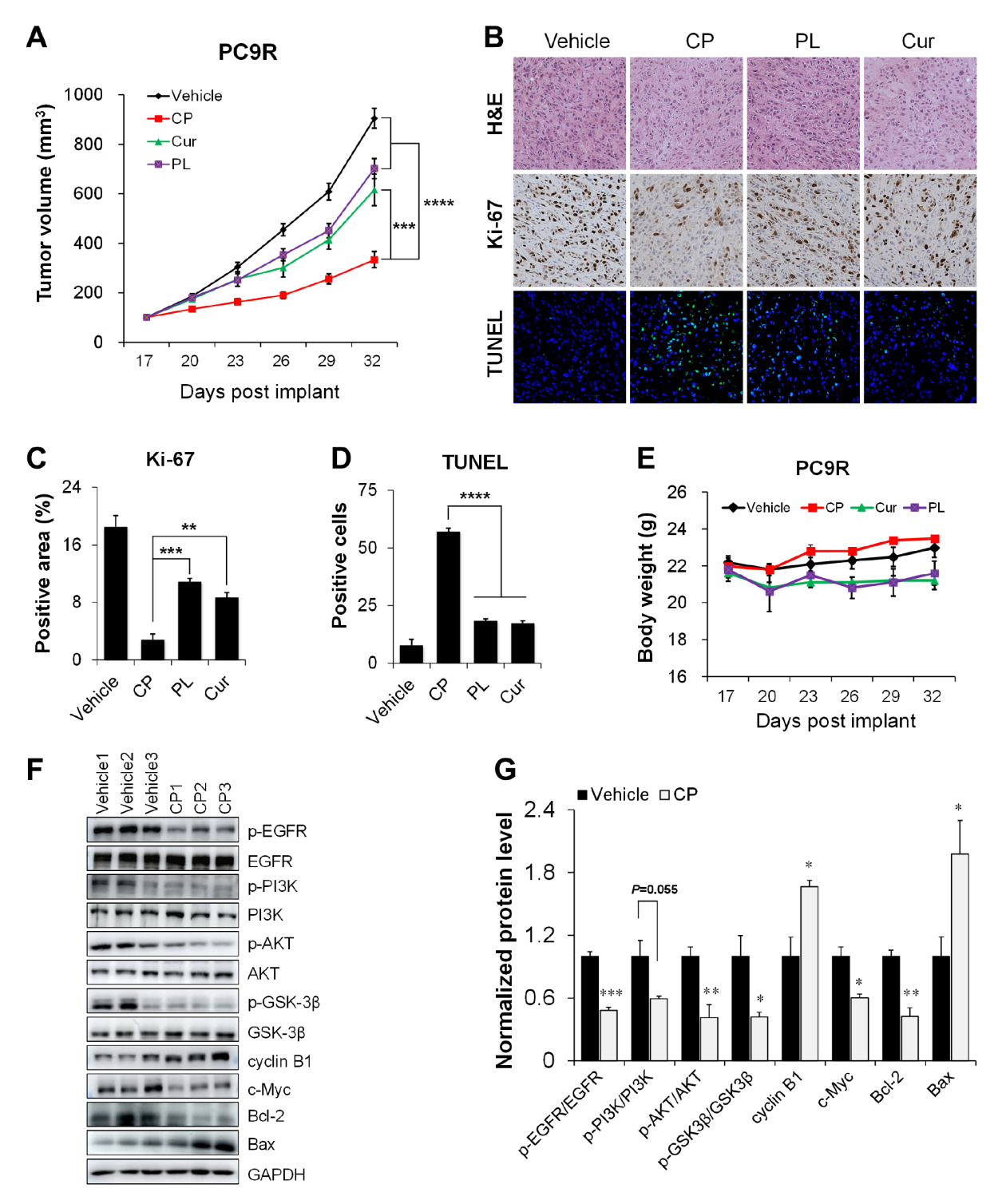


Figure 6. The effect of CP on EGFR-TKI-resistant lung cancer in xenograft tumors

Tumor-bearing mice were intraperitoneally injected with the Vehicle, CP (50 mg/kg), Cur (50 mg/kg), or PL (50 mg/kg). (A) Tumor volume of PC9R human lung cancer xenografts in nude mice (n = 8). (B) Tumor sections were analyzed by H&E, Ki-67 and TUNEL staining (200×). (C,D) Quantification of Ki-67 (C) and TUNEL (D) staining data. (E) Body weights of the tumor-bearing mice. (F) Proteins were extracted from tumor sections and subject to immunoblotting. (G) Quantified results of (F). Data are expressed as the mean \pm SE. *P < 0.05; **P < 0.01; ****P < 0.001; ****P < 0.0001.

Correspondingly, western blot analysis revealed that CP greatly inhibited the phosphorylation of EGFR, PI3K, AKT and GSK-3β. Moreover, the growth inhibition effect of CP on AZD9291-resistant lung cancer was further investigated *in vitro* and *in vivo*. Compared

with the parent compounds, treatment with CP effectively inhibited the growth and induced cell apoptosis in drug-resistant NSCLC cells. All these results suggest that GP can effectively overcome EGFR-TKI resistance.

The main acquired resistance mechanisms of 3rd generation EGFR-TKIs include changes in EGFR signaling pathway, aberrant activation of bypass and downstream signaling pathways, and histological transformation [28]. PPI network analysis revealed that the key target of intersect genes are EGFR, SRC, PIK3R, PIK3CA, KDR, MET, GRB2, PIK3CB, HSP90AA1, ITGB1. What's more, KEGG pathway analysis suggested that key pathway of intersect genes is the PI3K/AKT signaling pathway. Therefore, CP could reverse AZD9291 resistance though inhibition of EGFR and PI3K/AKT pathway. Recent study has shown that SRPK1 promotes gefitinib resistance by enhancing the autophosphorylation of GSK3β at Ser9 in NSCLC [29]. However, AKT blocking failed to inhibit the phosphorylation of GSK3β in SRPK1-overexpressing cell lines, suggesting that SRPK1-induced gefitinib resistance may be independent of the PI3K/AKT pathway. Our data suggested that both EGFR-AKT signaling cascade and GSK3ß activity were suppressed with CP administration. Nevertheless, whether GSK3β inhibition is independent of EGFR-AKT still needs further investigation.

In summary, this study combined network pharmacology and animal experiments to reveal that CP significantly suppress the growth of EGFR-TKI-resistant lung cancer cells by downregulating the EGFR/PI3K/AKT signaling cascade, providing a solid theoretical basis for the use of CP as a new therapeutic drug for advanced NSCLC.

Supplementary Data

Supplementary data is available at *Acta Biochimica et Biophysica Sinica* online.

Acknowledgement

We thank Scientific Research Center of Wenzhou Medical University for providing excellent consultation and instrumental supports.

Funding

This work was supported by the grants from the National Natural Science Foundation of China (No. 82203839 and 82273788) and the Natural Science Foundation of Zhejiang Province (No. LQ21H310007).

Conflict of Interest

The authors declare that they have no conflict of interest.

References

- Bray F, Laversanne M, Sung H, Ferlay J, Siegel RL, Soerjomataram I, Jemal A. Global cancer statistics 2022: GLOBOCAN estimates of incidence and mortality worldwide for 36 cancers in 185 countries. *CA Cancer J Clin* 2024, 74: 229–263
- Testa U, Castelli G, Pelosi E. Lung cancers: molecular characterization, clonal heterogeneity and evolution, and cancer stem cells. *Cancers* 2018, 10: 248
- da Cunha Santos G, Shepherd FA, Tsao MS. EGFR mutations and lung cancer. Annu Rev Pathol Mech Dis 2011, 6: 49–69
- Roskoski Jr. R. Small molecule inhibitors targeting the EGFR/ErbB family of protein-tyrosine kinases in human cancers. *Pharmacol Res* 2019, 139: 395–411
- Leonetti A, Sharma S, Minari R, Perego P, Giovannetti E, Tiseo M. Resistance mechanisms to osimertinib in EGFR-mutated non-small cell lung cancer. *Br J Cancer* 2019, 121: 725–737

- Soria JC, Ohe Y, Vansteenkiste J, Reungwetwattana T, Chewaskulyong B, Lee KH, Dechaphunkul A, et al. Osimertinib in untreated EGFR-mutated advanced non-small-cell lung cancer. N Engl J Med 2018, 378: 113–125
- Giordano A, Tommonaro G. Curcumin and cancer. Nutrients 2019, 11: 2376
- Wan Mohd Tajuddin WNB, Lajis NH, Abas F, Othman I, Naidu R. Mechanistic understanding of curcumin's therapeutic effects in lung cancer. Nutrients 2019, 11: 2989
- Parama D, Rana V, Girisa S, Verma E, Daimary UD, Thakur KK, Kumar A, et al. The promising potential of piperlongumine as an emerging therapeutics for cancer. Explor Targeted Anti-tumor Ther 2021, 2: 323– 354
- Miyazaki K, Morine Y, Xu C, Nakasu C, Wada Y, Teraoku H, Yamada S, et al. Curcumin-mediated resistance to lenvatinib via EGFR signaling pathway in hepatocellular carcinoma. Cells 2023, 12: 612
- 11. Chen P, Huang HP, Wang Y, Jin J, Long WG, Chen K, Zhao XH, et al. Curcumin overcome primary gefitinib resistance in non-small-cell lung cancer cells through inducing autophagy-related cell death. J Exp Clin Cancer Res 2019, 38: 254
- Wada K, Lee JY, Hung HY, Shi Q, Lin L, Zhao Y, Goto M, et al. Novel curcumin analogs to overcome EGFR-TKI lung adenocarcinoma drug resistance and reduce EGFR-TKI-induced GI adverse effects. Bioorg Med Chem 2015, 23: 1507–1514
- Karki K, Hedrick E, Kasiappan R, Jin UH, Safe S. Piperlongumine induces reactive oxygen species (ROS)-dependent downregulation of specificity protein transcription factors. *Cancer Prev Res* 2017, 10: 467–477
- Kang Q, Yan S. Piperlongumine reverses doxorubicin resistance through the PI3K/Akt signaling pathway in K562/A02 human leukemia cells. *Exp Ther Med* 2015, 9: 1345–1350
- 15. Zhang C, He LJ, Zhu YB, Fan QZ, Miao DD, Zhang SP, Zhao WY, et al. Piperlongumine inhibits Akt phosphorylation to reverse resistance to cisplatin in human non-small cell lung cancer cells via ROS regulation. Front Pharmacol 2019, 10: 1178
- Zhang Q, Hui M, Chen G, Huang H, Wang S, Ye Y, Wang Y, et al. Curcumin-piperlongumine hybrid molecule increases cell cycle arrest and apoptosis in lung cancer through JNK/c-jun signaling pathway. J Agric Food Chem 2024, 72: 7244–7255
- 17. Gong D, Yuan T, Wang R, Sun S, Dawuti A, Wang S, Du G, et al. Network pharmacology approach and experimental verification of Dan-Shen Decoction in the treatment of ischemic heart disease. *Pharm Biol* 2023, 61: 69–79
- Lu Z, Huang M, Lin H, Wang G, Li H. Network pharmacology and molecular docking approach to elucidate the mechanisms of Liuwei Dihuang pill in diabetic osteoporosis. *J Orthop Surg Res* 2022, 17: 314
- Luo J, Chen X, Liang P, Zhao Z, Wu T, Li Z, Wan S, et al. Mechanism of anti-hyperuricemia of isobavachin based on network pharmacology and molecular docking. Comput Biol Med 2023, 155: 106637
- Zhang G, Li Q, Chen Q, Su S. Network pharmacology: a new approach for chinese herbal medicine research. *Evid Based Complement Alternat Med* 2013, 2013: 1–9
- Kim MH, Bok M, Lim H, Yang WM. An integrative study on the inhibition
 of bone loss via osteo-F based on network pharmacology, experimental
 verification, and clinical trials in postmenopausal women. *Cells* 2023, 12:
 1992
- Ye X S, Osmani S A. Regulation of p34cdc2/cyclinB H1 and NIMA kinases during the G2/M transition and checkpoint responses in Aspergillus nidulans. *Prog Cell Cycle Res* 1997, 3: 221–232
- 23. Wang Z, Fan M, Candas D, Zhang TQ, Qin L, Eldridge A, Wachsmann-Hogiu S, *et al.* Cyclin B1/Cdk1 coordinates mitochondrial respiration for

- cell-cycle G2/M progression. Dev Cell 2014, 29: 217-232
- 24. Sun J, Du Y, Song Q, Nan J, Guan P, Guo J, Wang X, et al. E2F is required for STAT3-mediated upregulation of cyclin B1 and Cdc2 expressions and contributes to G2-M phase transition. Acta Biochim Biophys Sin 2019, 51: 313–322.
- Lindqvist A, Rodríguez-Bravo V, Medema RH. The decision to enter mitosis: feedback and redundancy in the mitotic entry network. *J Cell Biol* 2009, 185: 193–202
- Mok TS, Wu YL, Ahn MJ, Garassino MC, Kim HR, Ramalingam SS, Shepherd FA, et al. Osimertinib or platinum-pemetrexed in EGFR T790Mpositive lung cancer. N Engl J Med 2017, 376: 629–640
- 27. Wu YL, Cheng Y, Zhou X, Lee KH, Nakagawa K, Niho S, Tsuji F, *et al.*Dacomitinib versus gefitinib as first-line treatment for patients with EGFR-mutation-positive non-small-cell lung cancer (ARCHER 1050): a randomised, open-label, phase 3 trial. *Lancet Oncol* 1050, 18: 1454–1466
- 28. He J, Huang Z, Han L, Gong Y, Xie C. Mechanisms and management of 3rd-generation EGFR-TKI resistance in advanced non-small cell lung cancer (Review). *Int J Oncol* 2021, 59: 90
- 29. Huang JQ, Duan LX, Liu QY, Li HF, Hu AP, Song JW, Lin C, *et al.* Serine-arginine protein kinase 1 (SRPK1) promotes EGFR-TKI resistance by enhancing GSK3β Ser9 autophosphorylation independent of its kinase activity in non-small-cell lung cancer. *Oncogene* 2023, 42: 1233–1246